

Gauge dependence of on-shell and pole mass renormalization prescriptions

Yong Zhou

*Institute of High Energy Physics, Academia Sinica,
P.O. Box 918(4), Beijing 100049, China, Email: zhouy@ihep.ac.cn*

We discuss the gauge dependence of unstable boson's mass definition and physical result under the conventional on-shell mass renormalization prescription and the recently proposed pole mass renormalization prescription in standard model. By two-loop calculations we strictly prove that the on-shell mass renormalization prescription makes unstable boson's mass definition and the physical result gauge dependent, while we don't find such gauge dependence in the pole mass renormalization prescription. Besides, our calculation also shows the difference of the physical result between the two mass renormalization prescriptions cannot be neglected at two-loop level. Therefore we should use the pole mass renormalization prescription rather than the on-shell mass renormalization prescription to calculate physical results beyond one-loop level.

PACS numbers: 11.10.Gh, 12.15.Lk

I. INTRODUCTION

The conventional on-shell mass renormalization prescription has been present for a long time, in which the real part of particle's inverse propagator is renormalized to zero at physical mass point. For boson this is [1, 2]

$$m^2 - m_0^2 + \text{Re } \Sigma(m^2) = 0, \quad (1)$$

with m_0 the bare mass and Σ the boson's diagonal self energy (for vector boson it is the transverse self energy). But recently people proposed a new mass renormalization prescription which renormalizes both the real part and the imaginary part of the particle's inverse propagator to zero at the particle propagator's complex pole, i.e. [3, 4]

$$\bar{s} - m_0^2 + \Sigma(\bar{s}) = 0, \quad (2)$$

with \bar{s} the location of the particle propagator's complex pole. Written $\bar{s} = m_2^2 - im_2\Gamma_2$ the m_2 is defined as the physical mass in this mass renormalization prescription. Put the expression of \bar{s} into Eq.(2) one easily has [3, 4]

$$m_2^2 - m_0^2 + \text{Re } \Sigma(\bar{s}) = 0, \quad m_2 \Gamma_2 = \text{Im } \Sigma(\bar{s}). \quad (3)$$

After expanding Eqs.(3) about $\bar{s} = m_2^2$ one readily has from Eqs.(1,3) [3, 4]

$$m - m_2 = \Gamma_2 \text{Im } \Sigma'(m_2^2)/2 + O(g^6), \quad (4)$$

where $\Sigma'(m_2^2) = \partial \Sigma(m_2^2) / \partial p^2$ and g is a generic coupling constant. For unstable boson the r.h.s. of Eq.(4) is gauge dependent [3, 4]. So A. Sirlin et al. claim that the on-shell mass definition of unstable particles is gauge dependent basing on the conclusion that the location of the complex pole of unstable particle's propagator is gauge independent [3, 4, 5, 6].

We note that the conclusion that the location of the complex pole of unstable particle's propagator is gauge independent at any order in perturbation theory is only a native hypothesis and a strict proof of the hypothesis hasn't been present [7]. So whether the on-shell mass definition is gauge dependent still needs further investigation. In this paper we mainly investigate whether unstable boson's mass definition is gauge dependent under the on-shell and pole mass renormalization prescriptions. The arrangement is as follows: we firstly discuss the gauge dependence of the definitions of gauge boson W and Z's masses and the sine of the weak mixing angle under the two mass renormalization prescriptions; then we discuss the gauge dependence of the two-loop cross section of the physical process $\mu \rightarrow \nu_\mu e^- \bar{\nu}_e$ under the on-shell mass renormalization prescriptions; Lastly we give the conclusion.

II. GAUGE DEPENDENCE OF PHYSICAL PARAMETERS' DEFINITIONS UNDER THE ON-SHELL AND POLE MASS RENORMALIZATION PRESCRIPTIONS

If physical parameter is defined gauge independently, its counterterm must be also gauge independent [8]. This can be used to test whether the physical parameter's definition is gauge independent. In the follows we will investigate whether the definitions of gauge boson W and Z's masses and the sine of the weak mixing angle are gauge independent

under the on-shell and pole mass renormalization prescriptions. For convenience we only consider W gauge parameter's dependence in the R_ξ gauge and only introduce physical parameter's counterterms. The computer program packages *FeynArts* and *FeynCalc* [9] have been used in the following calculations. Note that there are some early two-loop calculations about the massive gauge boson's self energies [10].

From Eqs.(1,3) one easily has for massive boson [11]

$$\begin{aligned}\delta m^2 &= \text{Re } \Sigma(m^2), \\ \delta m_2^2 &= \text{Re } \Sigma(m_2^2) + m_2 \Gamma_2 \text{Im } \Sigma'(m_2^2) + \mathcal{O}(g^6).\end{aligned}\quad (5)$$

The W and Z one-loop mass counterterms have been proven gauge independent [6], so we only need to discuss the two-loop case. For convenience we only discuss the gauge dependence of the branch cut of W and Z two-loop mass counterterms. Since the gauge-dependent branch cut of massive boson's two-loop mass counterterm comprises gauge-dependent Heaviside functions only (see below) and the other part of massive boson's two-loop mass counterterm doesn't contain such functions, this simplified treatment is reasonable and will not break our final conclusion. The branch cut of W and Z two-loop mass counterterm will be calculated by the *cutting rules* [12, 13]. The concrete algorithm used here can be found in Ref.[13]. From Eqs.(5) we find the massive boson's two-loop mass counterterms are different in the two mass renormalization prescriptions. So we will calculate their gauge dependences separately in the follows.

We firstly discuss the gauge dependence of the branch cut of W two-loop mass counterterm under the on-shell mass renormalization prescription. Obviously we need to calculate the branch cut of W two-loop self energy. The W two-loop self energy can be classified into two kinds: one contains one-loop counterterms, the other doesn't contain any counterterm. Since except for CKM matrix elements [14] all the one-loop physical parameter's counterterms are real numbers and free of branch cut [2], the first kind self energy doesn't contribute to the branch cut of W two-loop mass counterterm, because except the one-loop counterterm the left part of the self energy is the one-loop self energy which real part is free of branch cut. Here we don't need to worry about the problem of the CKM matrix elements and their counterterms being complex numbers, because the total contribution of them to W two-loop mass counterterm is real number (see the following results for example). So we only need to consider the second kind self energy. According to the *cutting rules* of Ref.[13], the second kind self energy can also be classified into three kinds: one doesn't contain branch cut, the second contains branch cut, but its branch cut doesn't contribute to Eqs.(5), the third contains branch cut and its branch cut contributes to Eqs.(5). The topologies of the three kind self energies are separately shown in Fig.1-3. We note that in order to investigate the gauge dependence of gauge boson's mass counterterm the tadpole diagrams in Fig.1-2 must be included [6]. One also notices in Fig.1-3 that the one-particle-reducible diagrams have been included. Although a self energy is usually defined to comprise one-particle-irreducible diagrams only, no physical principle demonstrates that the one-particle-reducible diagram cannot be included in a correct self energy. Furthermore in the following calculations of gauge boson Z mass counterterm one will see the one-particle-reducible diagram in Fig.3 guarantees the branch cut of Z mass definition under the pole mass renormalization prescription is gauge independent. Obviously we only need to consider the contribution of Fig.3 to the branch cut of W two-loop mass counterterm. In Fig.3 we also draw the possible cuts of the first four topologies which contribute to W two-loop mass counterterm (the arrows on the inner lines denote the *positive-on-shell* momentum propagating directions of the cut propagators [13]). The possible cuts of the left two topologies which contribute to W two-loop mass counterterm are shown in Fig.4 and Fig.5. In the follows we will separately calculate the contributions of the possible cuts of Fig.3 to W two-loop mass counterterm.

In fact the cut of the first topology of Fig.3 doesn't contribute to W two-loop mass counterterm, since none of the Feynman diagrams of this topology contributes to W transverse self energy in standard model. For the second topology of Fig.3 there are 39 Feynman diagrams in electroweak standard model, but none of them satisfies the cutting condition or makes the cut contribution to W two-loop mass counterterm not equal to zero. The third topology of Fig.3 has the same conclusion as the second one. So we don't consider their contributions. For the 4th topology of Fig.3 the corresponding W self-energy diagrams which satisfy the cutting condition are shown in Fig.6. Using the cutting rules of Ref.[13] we obtain the contribution of the cuts of Fig.6 to W two-loop mass counterterm:

$$\text{Re } \Sigma_{WW}^T(m_W^2)|_{\xi_W-\text{cut}} = \frac{\alpha^2 m_W^2}{4608} (1 - \xi_W)^3 (\xi_W^5 - 3\xi_W^4 - 6\xi_W^3 - 46\xi_W^2 + 165\xi_W + 465) \theta[1 - \xi_W], \quad (6)$$

where Σ_{WW}^T is the W transverse self energy, m_W and ξ_W is W mass and gauge parameter, and the subscript $\xi_W-\text{cut}$ takes the ξ_W -dependent branch cut of the quantity, α is the fine structure constant, and θ is the Heaviside function. Here and forth we restrict ourselves to $\xi_W > 0$ [4].

For the 5th topology of Fig.3 the corresponding ξ_W -dependent W self-energy diagrams which cut contribution to W two-loop mass counterterm isn't equal to zero are shown in Fig.7. Using the cutting rules of Ref.[13] we obtain the

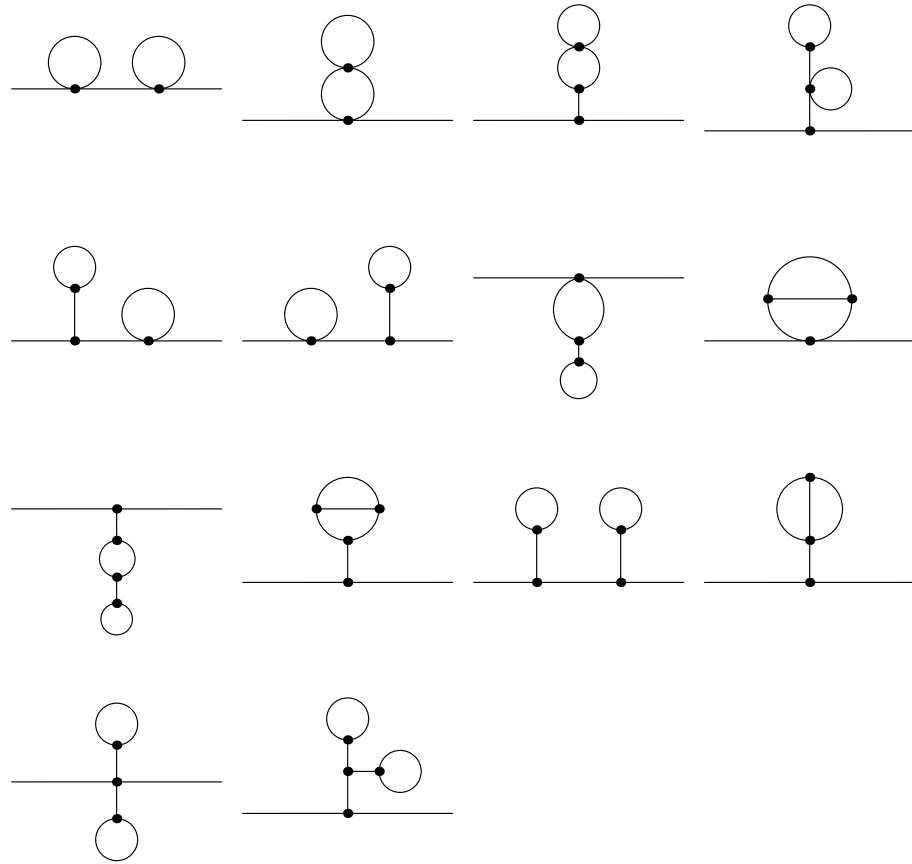


FIG. 1: Topologies of the two-loop self-energy diagrams without counterterm and branch cut.

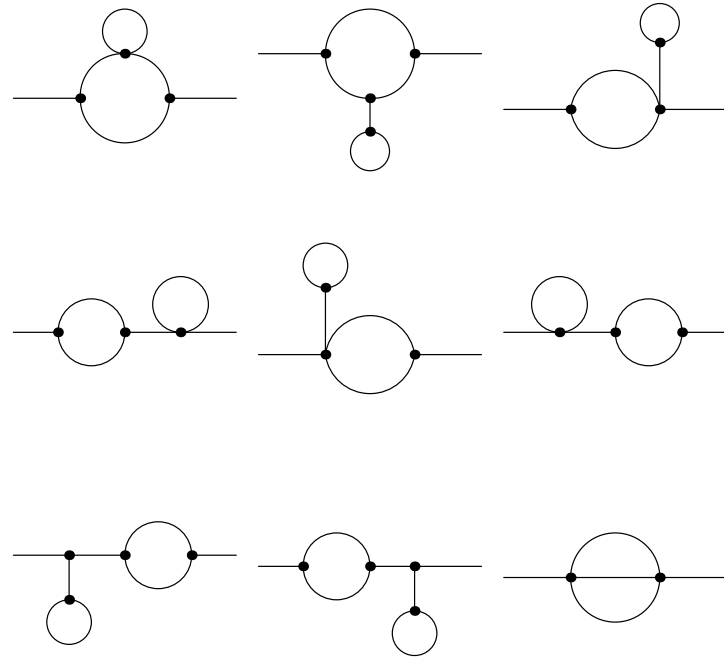


FIG. 2: Topologies of the two-loop self-energy diagrams without counterterm which branch cuts don't contribute to Eqs.(5).

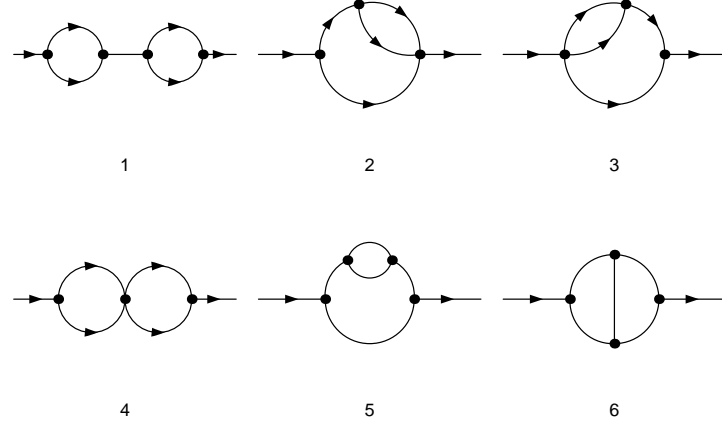


FIG. 3: Topologies of the two-loop self-energy diagrams without counterterm which branch cuts contribute to Eqs.(5).

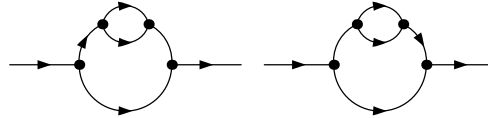


FIG. 4: Possible cuts of the 5th topologies of Fig.3 which contribute to Eqs.(5).

cut contribution of Fig.7 to W two-loop mass counterterm:

$$\begin{aligned}
 Re\Sigma_{WW}^T(m_W^2)|_{\xi_W-cut} = & \frac{\alpha^2 m_W^2}{128 s_w^4} \left[\sum_{i=e,\mu,\tau} \frac{1}{x_i} (1-x_i)(x_i - \xi_W)^2 (x_i^2 + x_i - 2) \theta[m_i - \sqrt{\xi_W} m_W] \right. \\
 & + \frac{1}{\xi_W^2} s_w^2 (1 - \xi_W)^3 \sum_{i=e,\mu,\tau} x_i (x_i - \xi_W)^2 \theta[\sqrt{\xi_W} m_W - m_i] \theta[1 - \xi_W] \\
 & + 3 \sum_{i=u,c} \sum_{j=d,s,b} \frac{1}{x_i} |V_{ij}|^2 (\xi_W - x_i + x_j) A_{ij} B_{ij} C_{ij} \theta[m_i - m_j - \sqrt{\xi_W} m_W] \\
 & \left. + 3 \sum_{i=u,c} \sum_{j=d,s,b} \frac{1}{x_j} |V_{ij}|^2 (\xi_W - x_j + x_i) A_{ij} B_{ij} C_{ij} \theta[m_j - m_i - \sqrt{\xi_W} m_W] \right]
 \end{aligned}$$

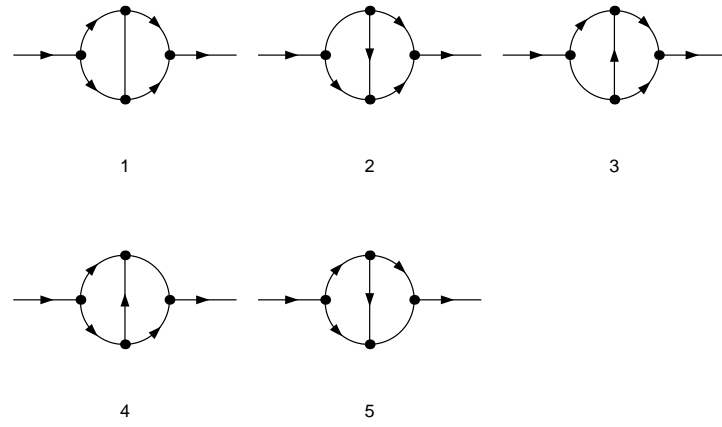


FIG. 5: Possible cuts of the 6th topologies of Fig.3 which contribute to Eqs.(5).

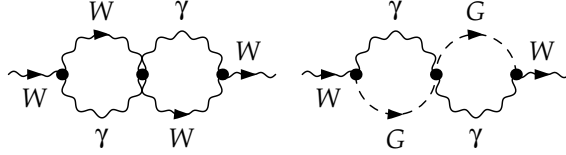


FIG. 6: W two-loop self-energy diagrams under the 4th topology of Fig.3 which satisfy the cutting condition.

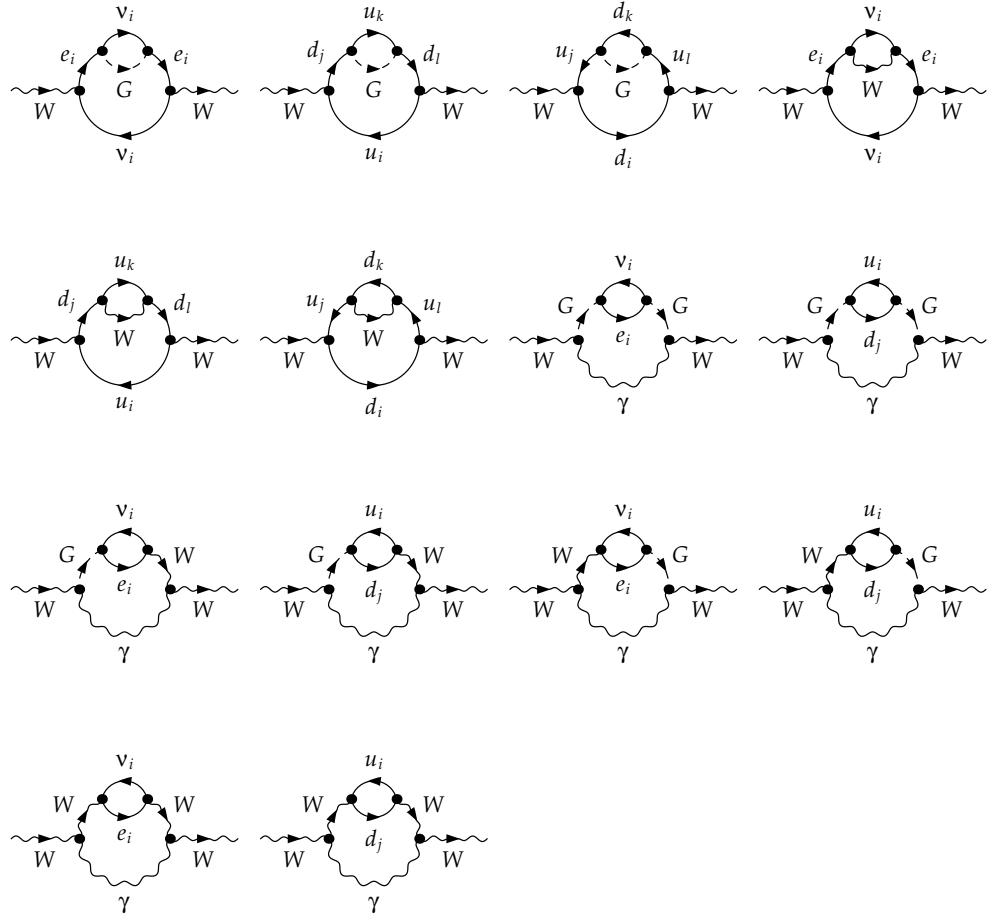


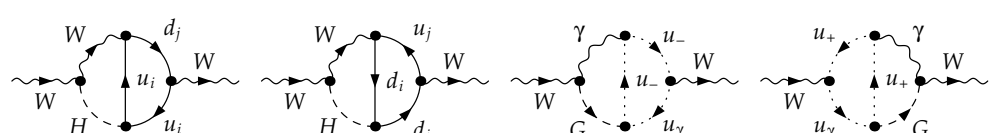
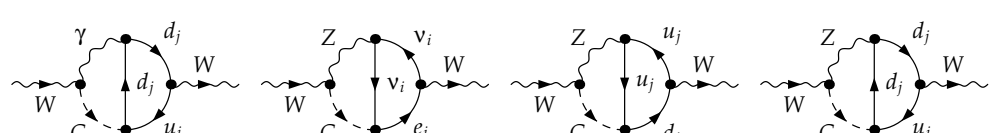
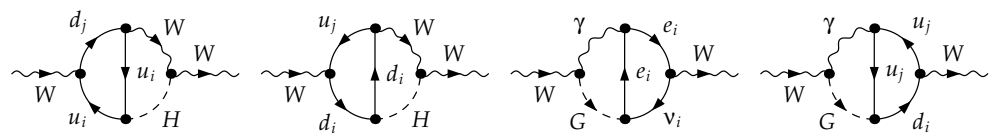
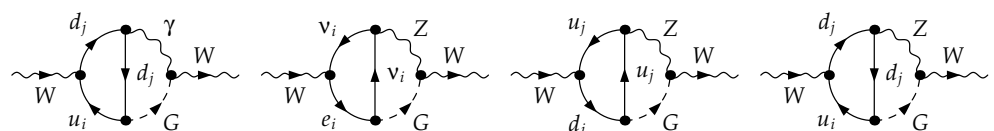
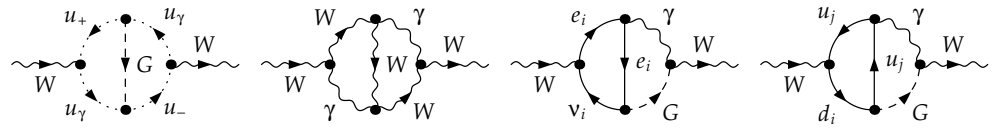
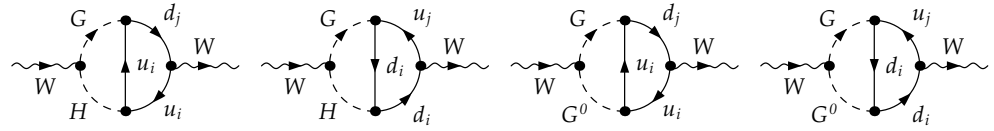
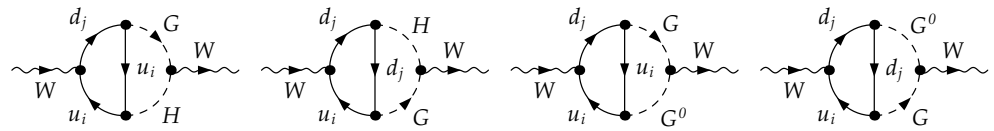
FIG. 7: W ξ_W -dependent two-loop self-energy diagrams under the 5th topology of Fig.3 which cut contribution to W two-loop mass counterterm isn't equal to zero.

$$\begin{aligned}
 & + \frac{3}{\xi_W^2} s_w^2 (1 - \xi_W)^3 \sum_{i=u,c} \sum_{j=d,s,b} |V_{ij}|^2 (\xi_W(x_i + x_j) - (x_i - x_j)^2) C_{ij} \\
 & \times \theta[\sqrt{\xi_W} m_W - m_i - m_j] \theta[1 - \xi_W] \Big] ,
 \end{aligned} \tag{7}$$

where s_w is the sine of the weak mixing angle, $x_i = m_i^2/m_W^2$, $x_j = m_j^2/m_W^2$, V_{ij} is the CKM matrix element [14], and

$$\begin{aligned}
 A_{ij} &= \sqrt{(x_i - x_j)^2 - 2(x_i + x_j) + 1}, \\
 B_{ij} &= 2 - (x_i + x_j) - (x_i - x_j)^2, \\
 C_{ij} &= \sqrt{(x_i - x_j)^2 - 2\xi_W(x_i + x_j) + \xi_W^2}.
 \end{aligned} \tag{8}$$

For the 6th topology of Fig.3 the corresponding ξ_W -dependent W self-energy diagrams which satisfy the cutting conditions of Fig.5 are shown in Fig.8. We will calculate the cut contributions of Fig.5 one by one. After carefully



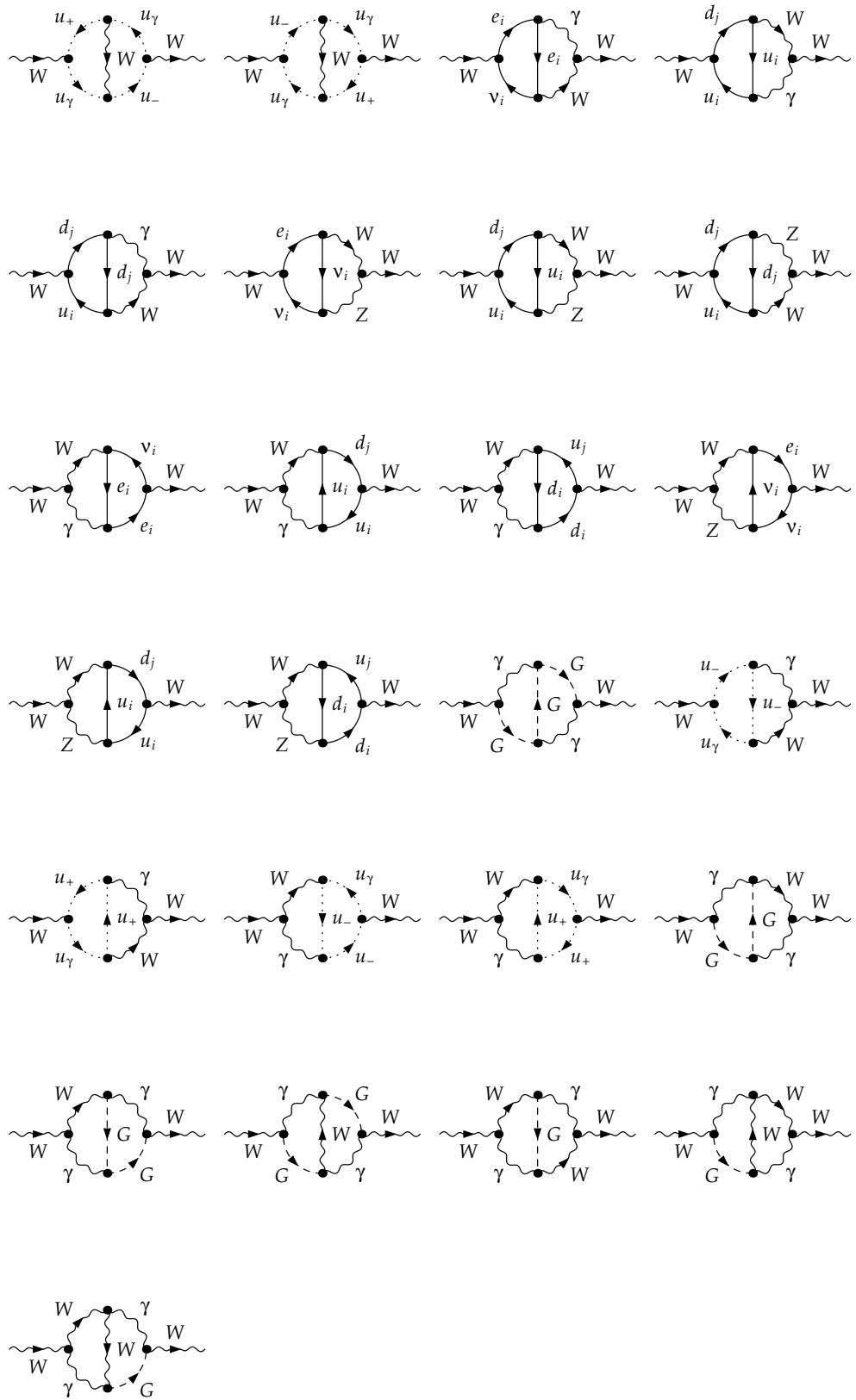


FIG. 8: $W \xi_W$ -dependent two-loop self-energy diagrams under the 6th topology of Fig.3 which satisfy the cutting conditions of Fig.5.

calculations we firstly obtain the contribution of the first cut of Fig.5 of the diagrams of Fig.8 to W two-loop mass counterterm:

$$\begin{aligned} Re\Sigma_{WW}^T(m_W^2)|_{\xi_W-cut} &= -\frac{\alpha^2 m_W^2}{576 s_w^2} \left[3 \sum_{i=u,c} \sum_{j=d,s,b} |V_{ij}|^2 A_{ij} B_{ij} + \sum_{i=e,\mu,\tau} (1-x_i)^2 (2+x_i) \right] (1-\xi_W)(\xi_W^2 - 2\xi_W - 11) \\ &\times \theta[1-\xi_W] - \frac{\alpha^2 m_W^2}{4608} (1-\xi_W)^3 (\xi_W^5 - 3\xi_W^4 - 6\xi_W^3 - 46\xi_W^2 + 165\xi_W + 465) \theta[1-\xi_W]. \end{aligned} \quad (9)$$

Then we obtain the contribution of the second and third cuts of Fig.5 of the diagrams of Fig.8 to W two-loop mass counterterm:

$$\begin{aligned} Re\Sigma_{WW}^T(m_W^2)|_{\xi_W-cut} &= -\frac{\alpha^2 m_W^2}{256 s_w^4} \left[\sum_{i=e,\mu,\tau} \frac{1}{x_i} (1-x_i)(x_i-\xi_W)^2 (x_i^2 + x_i - 2) \theta[m_i - \sqrt{\xi_W} m_W] \right. \\ &+ \frac{1}{\xi_W^2} s_w^2 (1-\xi_W)^3 \sum_{i=e,\mu,\tau} x_i (x_i-\xi_W)^2 \theta[\sqrt{\xi_W} m_W - m_i] \theta[1-\xi_W] \\ &+ 3 \sum_{i=u,c} \sum_{j=d,s,b} \frac{1}{x_i} |V_{ij}|^2 (\xi_W - x_i + x_j) A_{ij} B_{ij} C_{ij} \theta[m_i - m_j - \sqrt{\xi_W} m_W] \\ &+ 3 \sum_{i=u,c} \sum_{j=d,s,b} \frac{1}{x_j} |V_{ij}|^2 (\xi_W - x_j + x_i) A_{ij} B_{ij} C_{ij} \theta[m_j - m_i - \sqrt{\xi_W} m_W] \\ &+ \frac{3}{\xi_W^2} s_w^2 (1-\xi_W)^3 \sum_{i=u,c} \sum_{j=d,s,b} |V_{ij}|^2 (\xi_W(x_i + x_j) - (x_i - x_j)^2) C_{ij} \\ &\left. \times \theta[\sqrt{\xi_W} m_W - m_i - m_j] \theta[1-\xi_W] \right]. \end{aligned} \quad (10)$$

Through careful calculations we find the contribution of the 4th and 5th cuts of Fig.5 of the diagrams of Fig.8 to W two-loop mass counterterm is same as the one of the second and third cuts of Fig.5. This point can also be seen from the symmetry of the four cuts.

Summing up all of the above results (see Eqs.(5) and Eqs.(6,7,9,10)) we obtain the gauge dependence of the branch cut of W two-loop mass counterterm under the on-shell mass renormalization prescription

$$\delta m_W^2|_{\xi_W-cut} = -\frac{\alpha^2 m_W^2}{576 s_w^2} \left[3 \sum_{i=u,c} \sum_{j=d,s,b} |V_{ij}|^2 A_{ij} B_{ij} + \sum_{i=e,\mu,\tau} (1-x_i)^2 (2+x_i) \right] (1-\xi_W)(\xi_W^2 - 2\xi_W - 11) \theta[1-\xi_W]. \quad (11)$$

According to the above discussion below Eqs.(5) Eq.(11) proves the W two-loop mass counterterm is gauge dependent under the on-shell mass renormalization prescription. This means the conventional on-shell mass definition is gauge dependent according to the discussion at the beginning of this section.

Then we discuss the gauge dependence of the branch cut of W two-loop mass counterterm under the pole mass renormalization prescription. The calculations of the branch cut of W two-loop self energy are same as the case of the on-shell mass renormalization prescription. The other term in W two-loop mass counterterm is (see Eqs.(5))

$$\begin{aligned} m_W \Gamma_W \text{Im} \Sigma_{WW}^{T'}(m_W^2)|_{\xi_W-cut} &= \frac{\alpha^2 m_W^2}{576 s_w^2} \left[3 \sum_{i=u,c} \sum_{j=d,s,b} |V_{ij}|^2 A_{ij} B_{ij} + \sum_{i=e,\mu,\tau} (1-x_i)^2 (2+x_i) \right] \\ &\times (1-\xi_W)(\xi_W^2 - 2\xi_W - 11) \theta[1-\xi_W]. \end{aligned} \quad (12)$$

From the above results (see Eqs.(5) and Eqs.(6,7,9,10,12)) one readily has

$$\delta m_W^2|_{\xi_W-cut} = 0. \quad (13)$$

This means in W pole mass definition we don't find the gauge dependence present in W on-shell mass definition.

Similarly we can discuss the gauge dependence of Z mass definition under the on-shell and pole mass renormalization prescriptions. We also calculate the gauge dependence of the branch cut of Z two-loop mass counterterms only. Firstly we discuss the case of the on-shell mass renormalization prescription. According to the above discussions we only need to calculate the contributions of the branch cuts of Fig.3 to Z two-loop mass counterterm. In the follows we will separately calculate their contributions.

For the first topology of Fig.3 only the diagrams whose middle propagator is photon have contribution to Z transverse self energy. Through calculating the branch cut of Z-photon one-loop two-point function we obtain the ξ_W -dependent contribution of the branch cut of the first topology of Fig.3 to Z two-loop mass counterterm

$$\begin{aligned}
Re\Sigma_{ZZ}^T(m_Z^2)|_{\xi_W-cut} = & \frac{\alpha^2 m_W^2}{6912 c_w^6 s_w^2} (1 - 4 c_w^2 \xi_W)^{3/2} \left[\frac{3}{c_w^2} (1 - 4 c_w^2 \xi_W)^{3/2} + 8(3(4c_w^2 - 3) \sum_{i=e,\mu,\tau} + 2(8c_w^2 - 5) \sum_{i=u,c} \right. \\
& + (4c_w^2 - 1) \sum_{i=d,s,b}) \sqrt{1 - 4 c_w^2 x_i} (2 c_w^2 x_i + 1) \left. \right] \theta \left[\frac{1}{c_w} - 2\sqrt{\xi_W} \right] + \frac{\alpha^2 m_W^2}{1728 c_w^6} D E \\
& \times \left[\frac{3 s_w^2}{c_w^2} D E - \frac{3}{c_w^2} (1 - 4 c_w^2 \xi_W)^{3/2} - 4(3(4c_w^2 - 3) \sum_{i=e,\mu,\tau} + 2(8c_w^2 - 5) \sum_{i=u,c} + (4c_w^2 - 1) \sum_{i=d,s,b} \right. \\
& \left. \times \sqrt{1 - 4 c_w^2 x_i} (2 c_w^2 x_i + 1) \right] \theta \left[\frac{1}{c_w} - \sqrt{\xi_W} - 1 \right], \tag{14}
\end{aligned}$$

where m_Z is Z mass, c_w is the cosine of the weak mixing angle, and

$$\begin{aligned}
D &= \sqrt{(\xi_W - 1)^2 c_w^4 - 2(\xi_W + 1)c_w^2 + 1}, \\
E &= (\xi_W - 1)^2 c_w^4 - 2(\xi_W - 5)c_w^2 + 1. \tag{15}
\end{aligned}$$

For the second topology of Fig.3 there are four Z self-energy diagrams as shown in Fig.9 which branch-cut contribution to Z two-loop mass counterterm isn't equal to zero. By the cutting rules of Ref.[13] we obtain the contribution

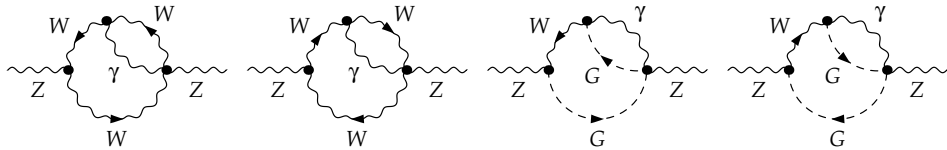


FIG. 9: Z two-loop self-energy diagrams under the second topology of Fig.3 which branch-cut contribution to Eqs.(5) isn't equal to zero.

of the cuts of Fig.9 to Z two-loop mass counterterm:

$$\begin{aligned}
Re\Sigma_{ZZ}^T(m_Z^2)|_{\xi_W-cut} = & \frac{\alpha^2 m_W^2}{1536 c_w^4} (\xi_W - 1) D \left[(\xi_W - 1)^3 (\xi_W^3 - \xi_W^2 - 3\xi_W - 33) c_w^6 \right. \\
& - (\xi_W - 1) (3\xi_W^4 - 9\xi_W^3 - 29\xi_W^2 + 101\xi_W + 366) c_w^4 \\
& \left. + (3\xi_W^4 - 10\xi_W^3 - 22\xi_W^2 + 170\xi_W - 93) c_w^2 - \xi_W^3 + 2\xi_W^2 + 5\xi_W - 18 \right] \theta \left[\frac{1}{c_w} - \sqrt{\xi_W} - 1 \right]. \tag{16}
\end{aligned}$$

For the third topology of Fig.3 there are also four Z self-energy diagrams as shown in Fig.10 which branch-cut contribution to Z two-loop mass counterterm isn't equal to zero. Obviously Fig.9 and Fig.10 are right-and-left

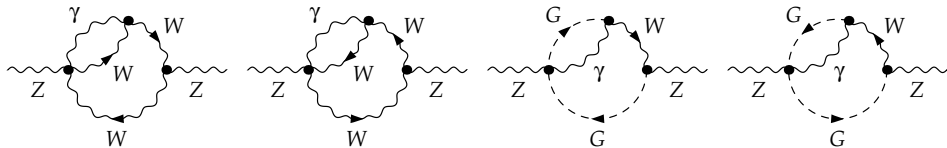


FIG. 10: Z two-loop self-energy diagrams under the third topology of Fig.3 which branch-cut contribution to Eqs.(5) isn't equal to zero.

symmetric. Through calculations we also find the contribution of the cuts of Fig.10 to Z two-loop mass counterterm is same as the one of Fig.9, i.e. Eq.(16).

For the 4th topology of Fig.3 there are six Z self-energy diagrams as shown in Fig.11 which branch-cut contribution to Z two-loop mass counterterm isn't equal to zero. After careful calculations we obtain the contribution of the cuts

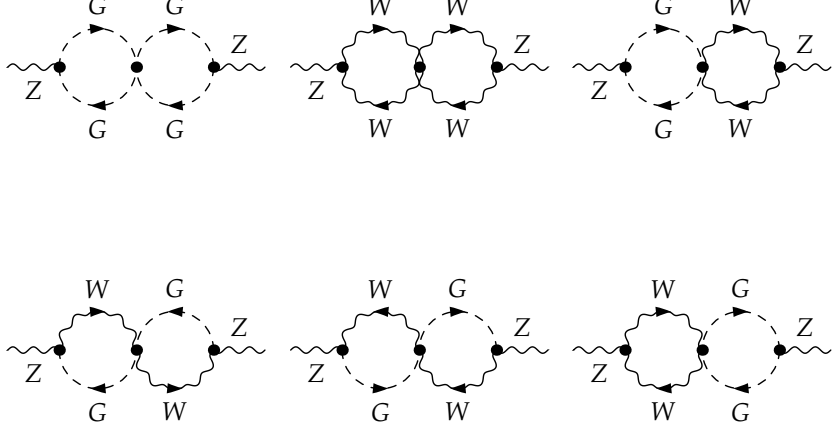


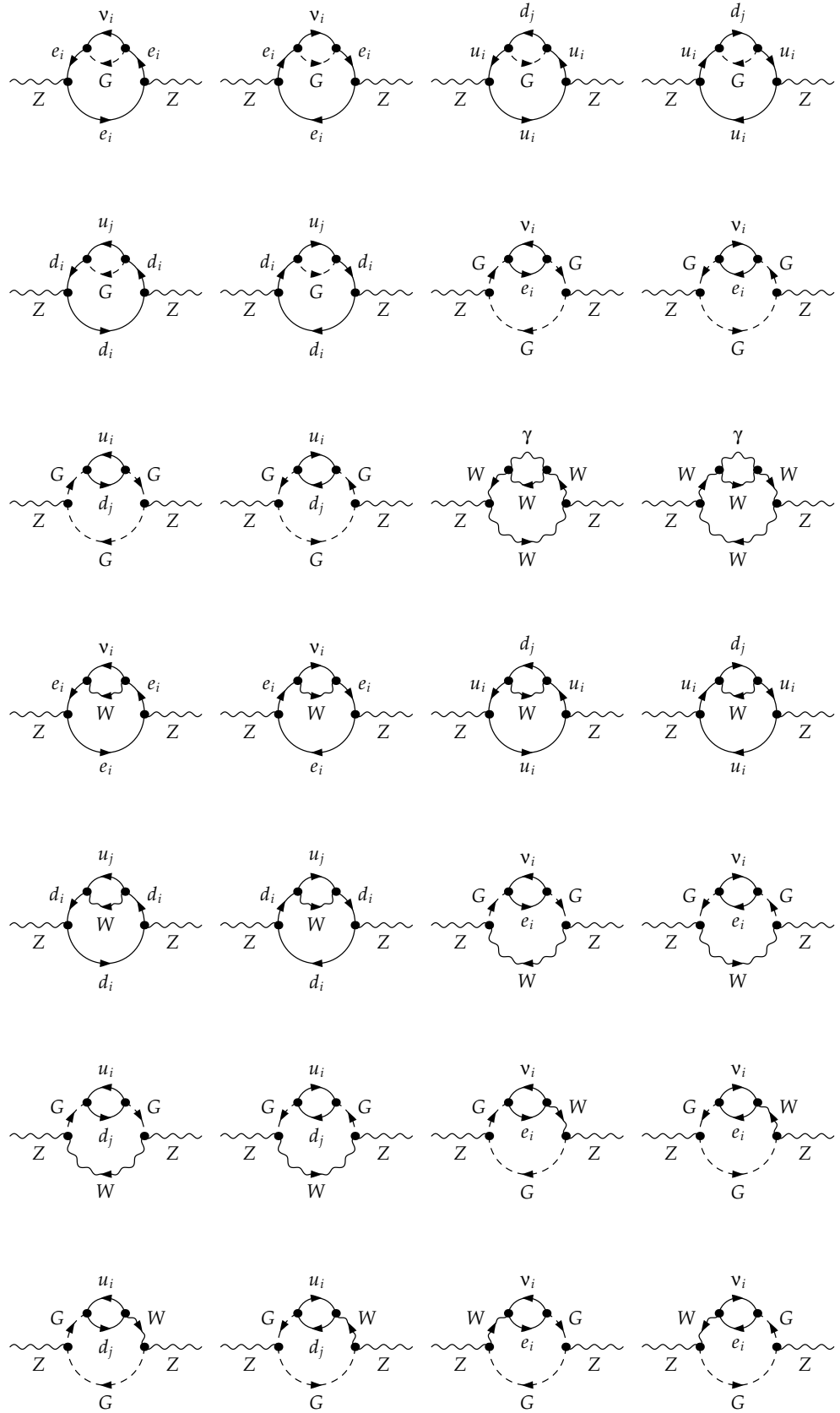
FIG. 11: Z two-loop self-energy diagrams under the 4th topology of Fig.3 which branch-cut contribution to Eqs.(5) isn't equal to zero.

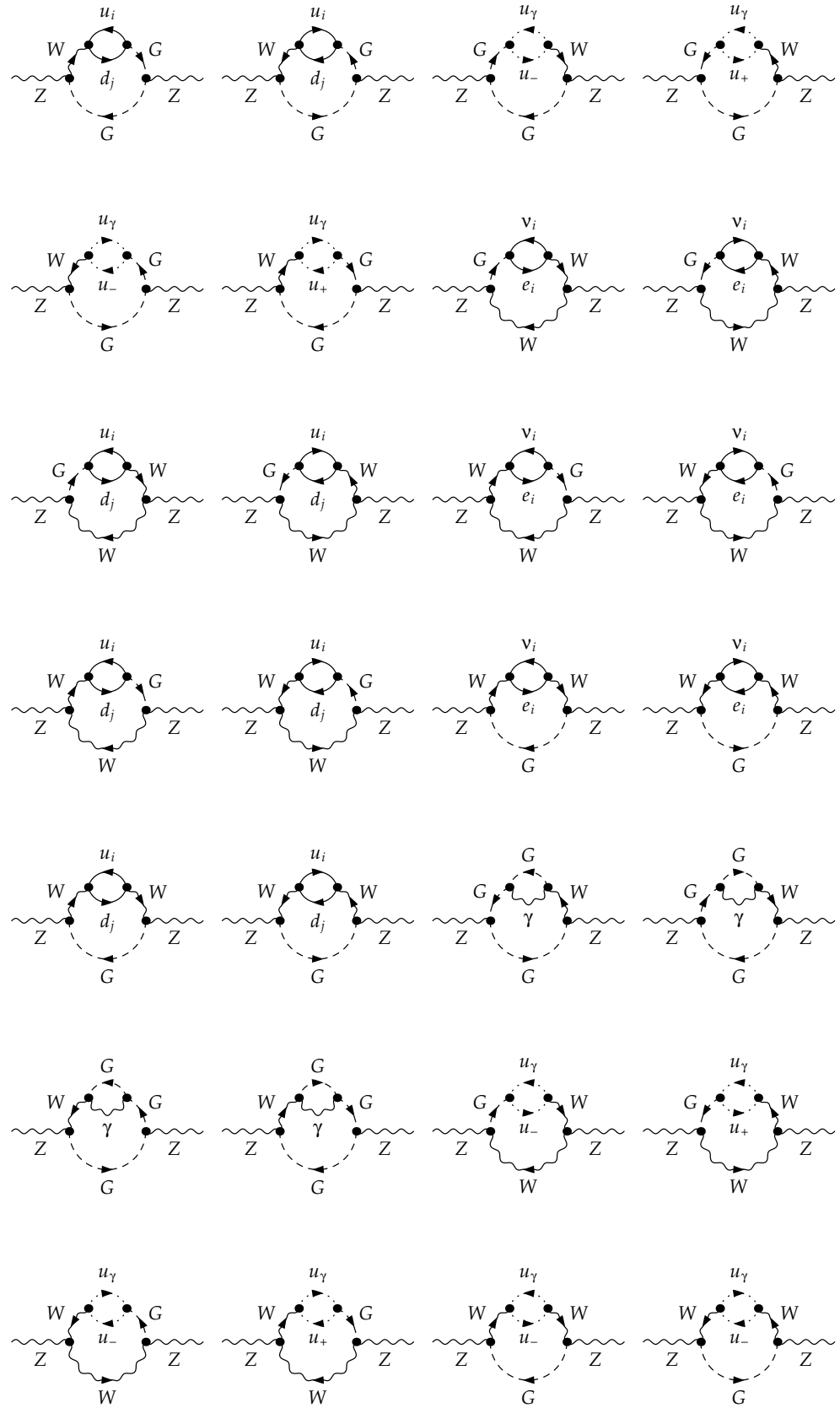
of Fig.11 to Z two-loop mass counterterm:

$$\begin{aligned}
 Re\Sigma_{ZZ}^T(m_Z^2)|_{\xi_W-cut} = & \frac{\alpha^2 m_W^2}{4608 c_w^8 s_w^4} (1 - 4 c_w^2 \xi_W)^3 (2 c_w^6 - 4 c_w^4 + 2 c_w^2 - 3) \theta\left[\frac{1}{c_w} - 2\sqrt{\xi_W}\right] \\
 & + \frac{\alpha^2 m_W^2}{2304 c_w^8} [(\xi_W - 1)^6 c_w^{14} - 6(\xi_W - 1)^4 (\xi_W^2 + 11\xi_W + 22) c_w^{12} \\
 & + 3(\xi_W - 1)^2 (12\xi_W^3 + 65\xi_W^2 + 10\xi_W + 201) c_w^{10} \\
 & - 2(45\xi_W^4 + 46\xi_W^3 - 228\xi_W^2 - 150\xi_W + 415) c_w^8 + 3(40\xi_W^3 - 19\xi_W^2 - 98\xi_W + 109) c_w^6 \\
 & - 6(15\xi_W^2 - 17\xi_W - 12) c_w^4 + (36\xi_W - 35) c_w^2 - 6] \theta\left[\frac{1}{c_w} - \sqrt{\xi_W} - 1\right] \\
 & - \frac{\alpha^2 m_W^2}{1152 c_w^8 s_w^2} D \sqrt{1 - 4 c_w^2 \xi_W} [4(\xi_W - 1)^2 \xi_W c_w^{10} - (4\xi_w^3 + \xi_W^2 - 38\xi_W + 1) c_w^8 \\
 & + 3(4\xi_W^3 + 19\xi_W^2 - 32\xi_W - 3) c_w^6 - 3(9\xi_W^2 - 10\xi_W - 8) c_w^4 \\
 & + (18\xi_W - 11) c_w^2 - 3] \theta\left[\frac{1}{c_w} - \sqrt{\xi_W} - 1\right]. \tag{17}
 \end{aligned}$$

For the 5th topology of Fig.3 there are 84 Z self-energy diagrams as shown in Fig.12 which branch-cut contribution to Z two-loop mass counterterm isn't equal to zero. By the cutting rules of Ref.[13] we obtain the contribution of the cuts of Fig.12 to Z two-loop mass counterterm:

$$\begin{aligned}
 Re\Sigma_{ZZ}^T(m_Z^2)|_{\xi_W-cut} = & \frac{\alpha^2 m_W^2}{192 c_w^2 s_w^2} D E \left[\sum_{i=e,\mu,\tau} (1 - x_i)^2 (2 + x_i) + 3 \sum_{i=u,c} \sum_{j=d,s,b} |V_{ij}|^2 A_{ij} B_{ij} \right] \theta\left[\frac{1}{c_w} - \sqrt{\xi_W} - 1\right] \\
 & + \frac{\alpha^2 m_W^2}{64 s_w^4 \xi_W^2} (1 - 4 c_w^2 \xi_W)^{3/2} \sum_{i=e,\mu,\tau} x_i (x_i - \xi_W)^2 \theta\left[\frac{1}{c_w} - 2\sqrt{\xi_W}\right] \theta[\sqrt{\xi_W} m_W - m_i] \\
 & + \frac{3 \alpha^2 m_W^2}{64 s_w^4 \xi_W^2} (1 - 4 c_w^2 \xi_W)^{3/2} \sum_{i=u,c} \sum_{j=d,s,b} |V_{ij}|^2 C_{ij} (\xi_W (x_i + x_j) - (x_i - x_j)^2) \\
 & \times \theta\left[\frac{1}{c_w} - 2\sqrt{\xi_W}\right] \theta[\sqrt{\xi_W} m_W - m_i - m_j] - \frac{\alpha^2 m_W^2}{64 c_w^4 s_w^4} (2 c_W^2 - 1) \sum_{i=e,\mu,\tau} \frac{1}{x_i} \sqrt{1 - 4 c_w^2 x_i} \\
 & \times (x_i - \xi_W)^2 (2 c_w^2 - 1 + c_w^2 (4 c_w^2 - 5) x_i) \theta[m_i - \sqrt{\xi_W} m_W] \\
 & + \frac{\alpha^2 m_W^2}{192 c_w^4 s_w^4} (4 c_W^2 - 1) \sum_{i=u,c} \sum_{j=d,s,b} \frac{1}{x_i} |V_{ij}|^2 C_{ij} \sqrt{1 - 4 c_w^2 x_i} (\xi_W - x_i + x_j) \\
 & \times (4 c_w^2 - 1 + c_w^2 (8 c_w^2 - 11) x_i) \theta[m_i - m_j - \sqrt{\xi_W} m_W]
 \end{aligned}$$





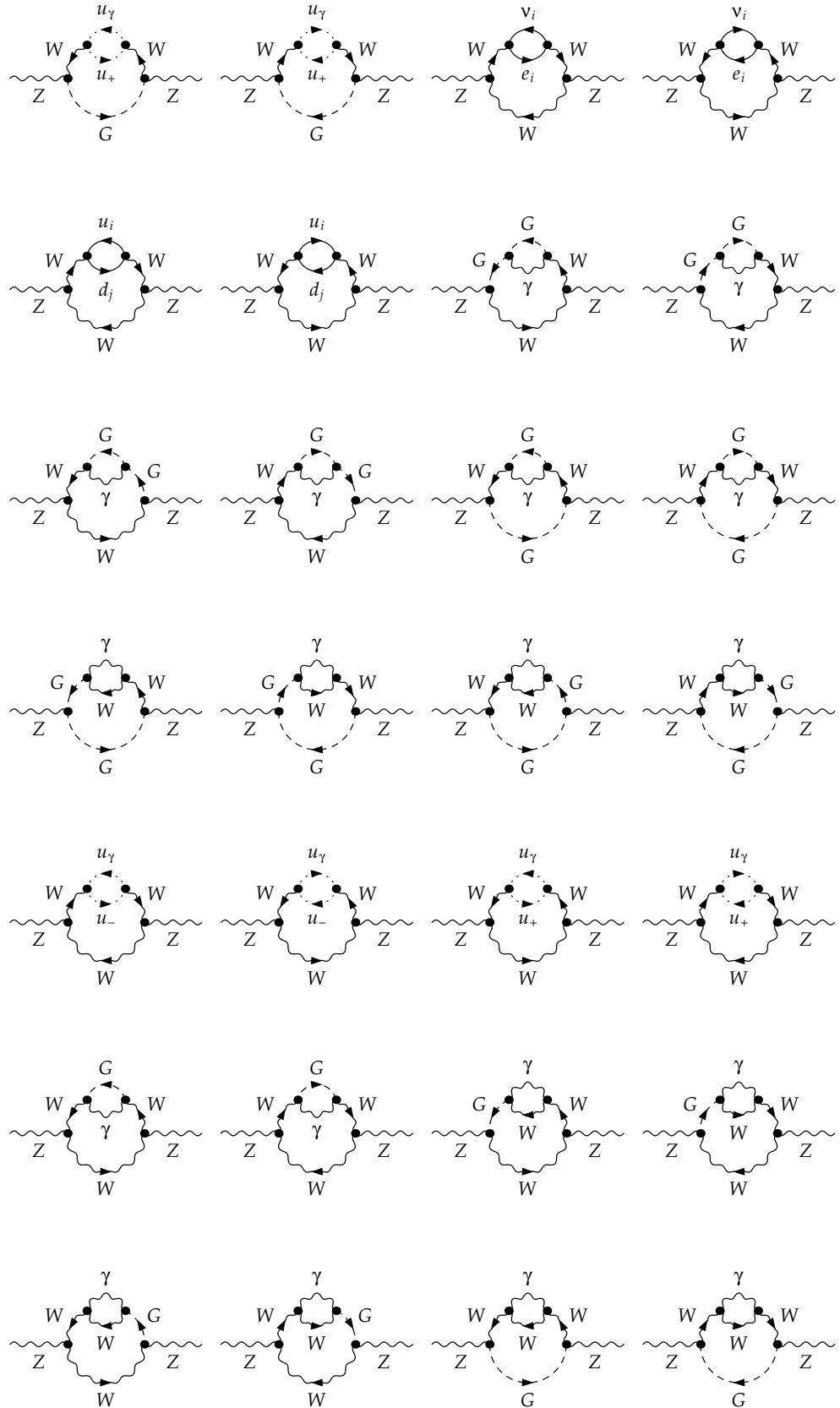


FIG. 12: Z two-loop self-energy diagrams under the 5th topology of Fig.3 which branch-cut contribution to Eqs.(5) isn't equal to zero.

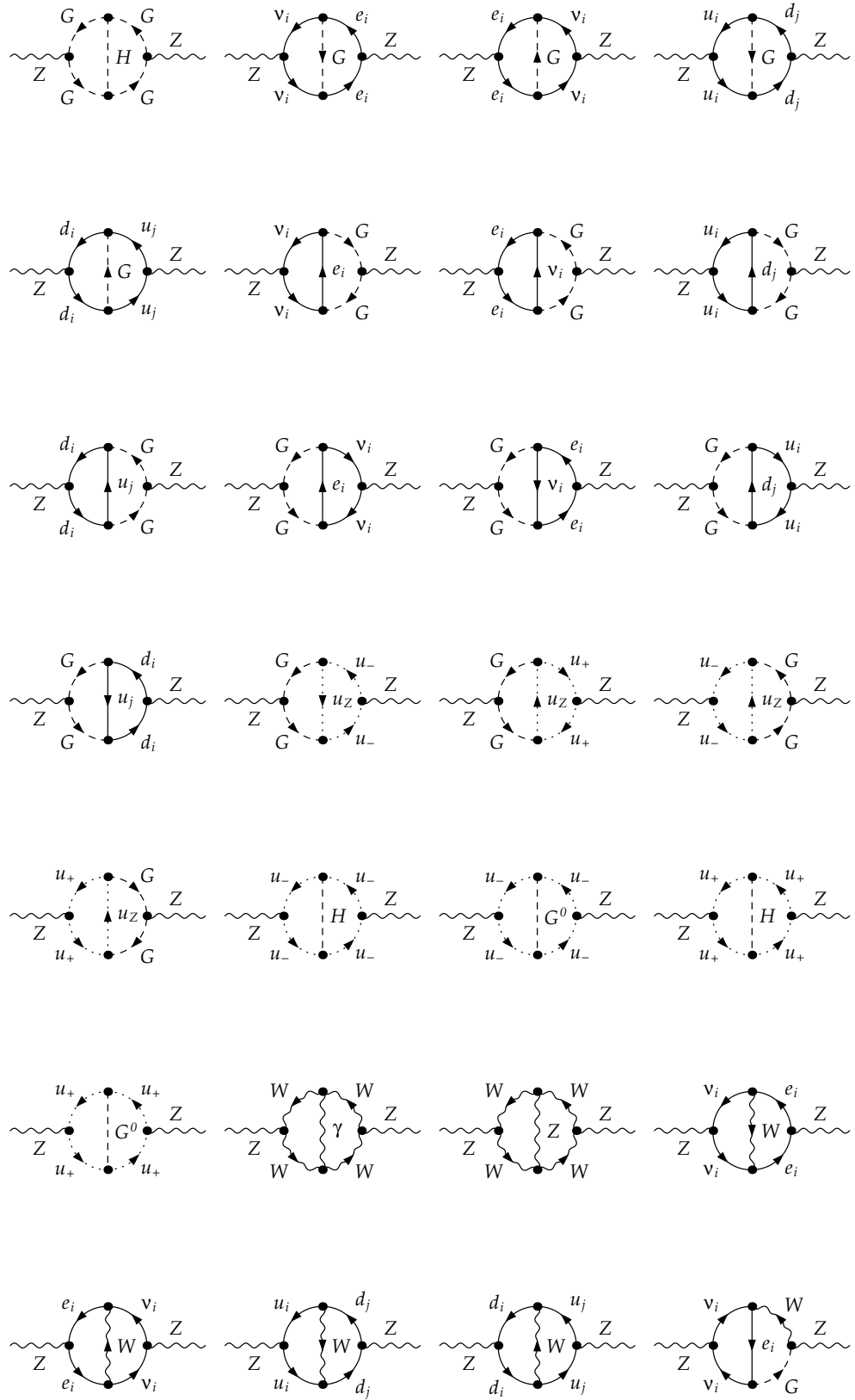
$$\begin{aligned}
& + \frac{\alpha^2 m_W^2}{192 c_w^4 s_w^4} (2c_W^2 + 1) \sum_{i=u,c} \sum_{j=d,s,b} \frac{1}{x_j} |V_{ij}|^2 C_{ij} \sqrt{1 - 4 c_w^2 x_j} (\xi_W - x_j + x_i) \\
& \times (2c_w^2 + 1 + c_w^2 (4c_w^2 - 7)x_j) \theta[m_j - m_i - \sqrt{\xi_W} m_W]. \tag{18}
\end{aligned}$$

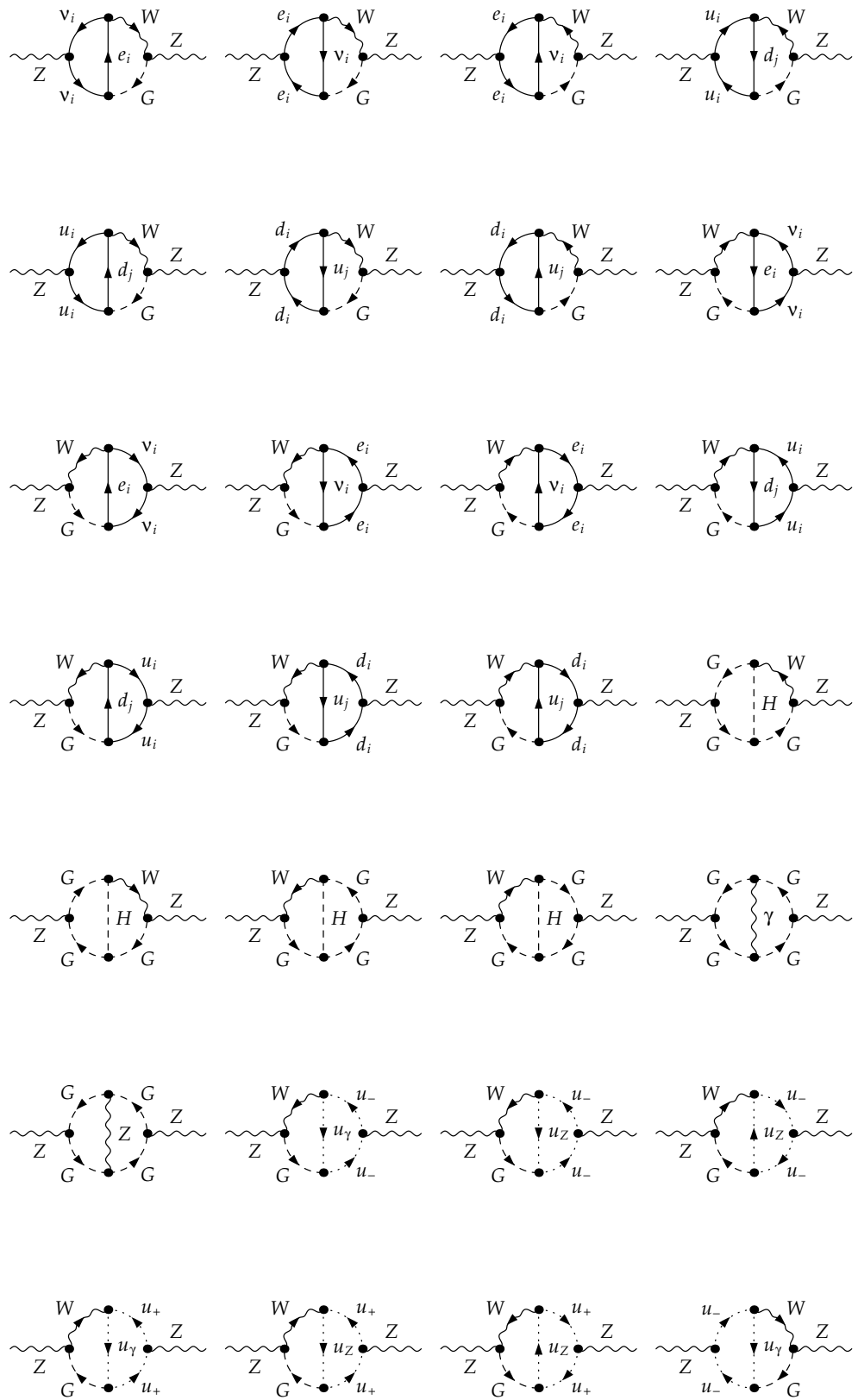
For the 6th topology of Fig.3 the corresponding ξ_W -dependent Z self-energy diagrams which satisfy the cutting conditions of Fig.5 are shown in Fig.13. We will calculate the cut contributions of Fig.5 one by one. After carefully calculations we firstly obtain the ξ_W -dependent contribution of the first cut of Fig.5 of the diagrams of Fig.13 to Z two-loop mass counterterm:

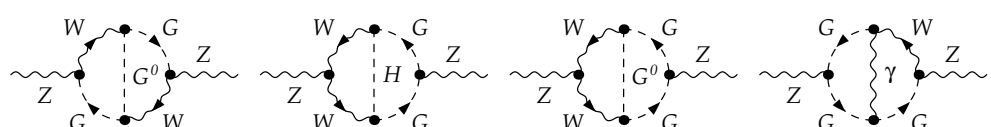
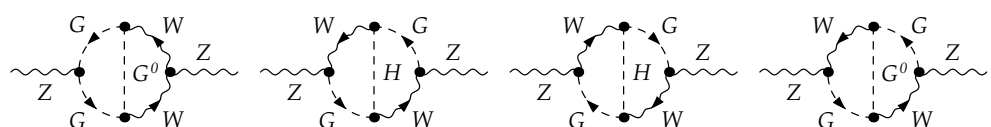
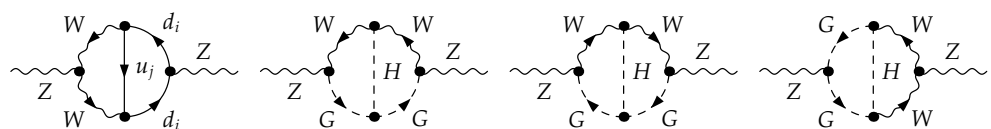
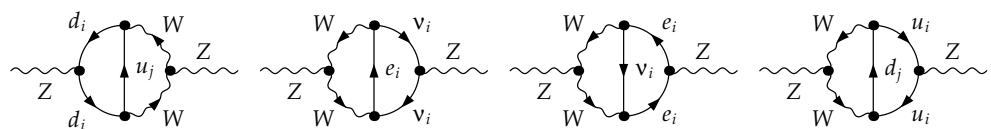
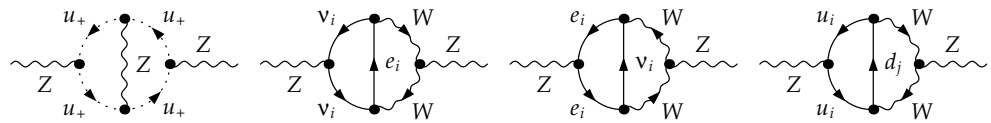
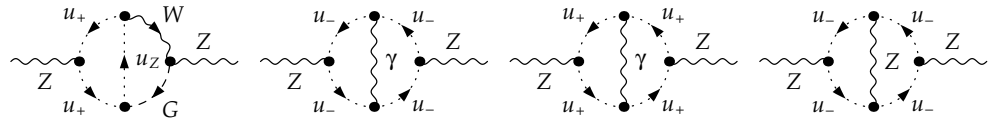
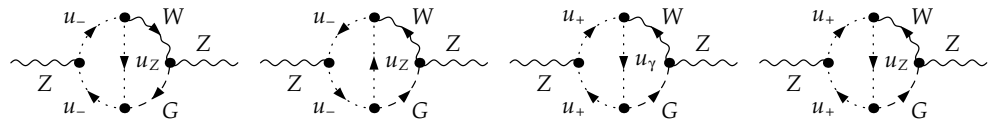
$$\begin{aligned}
Re\Sigma_{ZZ}^T(m_Z^2)|_{\xi_W-cut} = & \frac{\alpha^2 m_W^2}{4608 c_w^8 s_w^4} (1 - 4 c_w^2 \xi_W)^3 (1 + 4c_w^4 - 2c_w^6) \theta\left[\frac{1}{c_w} - 2\sqrt{\xi_W}\right] \\
& - \frac{\alpha^2 m_W^2}{576 c_w^6 s_w^4} (1 - 4 c_w^2 \xi_W)^{3/2} \left[3 + \left(\sum_{i=e,\mu,\tau} 2c_w^2 - 1 + c_w^2 (4c_w^2 - 5)x_i \right. \right. \\
& + \sum_{i=u,c} 4c_w^2 - 1 + c_w^2 (8c_w^2 - 11)x_i + \sum_{i=d,s,b} 2c_w^2 + 1 + c_w^2 (4c_w^2 - 7)x_i \\
& \times \left. \sqrt{1 - 4 c_w^2 x_i} \right) \theta\left[\frac{1}{c_w} - 2\sqrt{\xi_W}\right] + \frac{\alpha^2 m_W^2}{1152 c_w^8 s_w^2} D \sqrt{1 - 4 c_w^2 \xi_W} \\
& \times [4(\xi_W - 1)^2 \xi_W c_w^{10} + (4\xi_W^3 - 17\xi_W^2 + 46\xi_W - 1)c_w^8 + (4\xi_W^3 + 55\xi_W^2 - 20\xi_W - 11)c_w^6 \\
& - (9\xi_W^2 + 42\xi_W - 6)c_w^4 + (6\xi_W + 7)c_w^2 - 1] \theta\left[\frac{1}{c_w} - \sqrt{\xi_W} - 1\right] \\
& + \frac{\alpha^2 m_W^2}{2304 c_w^8} [3(\xi_W - 1)^6 c_w^{14} + 2(\xi_W - 1)^4 (\xi_W^2 + 25\xi_W + 100)c_w^{12} \\
& - 3(\xi_W - 1)^2 (4\xi_W^3 + 85\xi_W^2 + 58\xi_W + 141)c_w^{10} + 6(5\xi_W^4 + 74\xi_W^3 - 144\xi_W^2 - 50\xi_W - 13)c_w^8 \\
& - (40\xi_W^3 + 411\xi_W^2 - 798\xi_W - 581)c_w^6 + 6(5\xi_W^2 + 31\xi_W - 42)c_w^4 \\
& - 3(4\xi_W + 11)c_w^2 + 2] \theta\left[\frac{1}{c_w} - \sqrt{\xi_W} - 1\right] + \frac{\alpha^2 m_W^2}{288 c_w^6 s_w^2} D E \\
& \times [3 + \left(\sum_{i=e,\mu,\tau} (2c_w^2 - 1 + c_w^2 (4c_w^2 - 5)x_i) + \sum_{i=u,c} (4c_w^2 - 1 + c_w^2 (8c_w^2 - 11)x_i) \right. \\
& \left. + \sum_{i=d,s,b} (2c_w^2 + 1 + c_w^2 (4c_w^2 - 7)x_i) \right) \sqrt{1 - 4 c_w^2 x_i} \theta\left[\frac{1}{c_w} - \sqrt{\xi_W} - 1\right]. \tag{19}
\end{aligned}$$

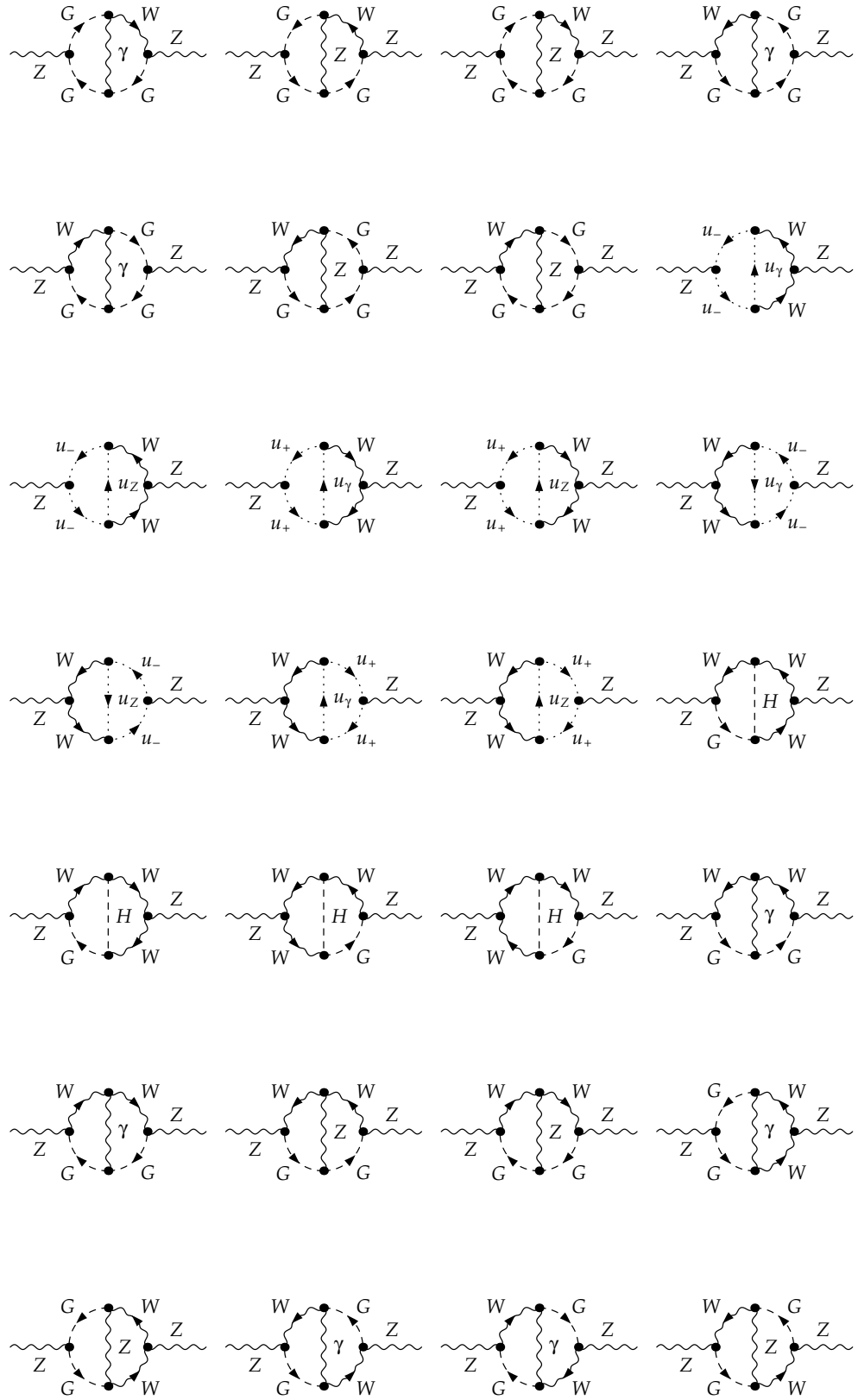
Then we obtain the ξ_W -dependent contribution of the second and third cuts of Fig.5 of the diagrams of Fig.13 to Z two-loop mass counterterm

$$\begin{aligned}
Re\Sigma_{ZZ}^T(m_Z^2)|_{\xi_W-cut} = & -\frac{\alpha^2 m_W^2}{384 c_w^2 s_w^2} D E \left[\sum_{i=e,\mu,\tau} (1 - x_i)^2 (2 + x_i) + 3 \sum_{i=u,c} \sum_{j=d,s,b} |V_{ij}|^2 A_{ij} B_{ij} \right] \theta\left[\frac{1}{c_w} - \sqrt{\xi_W} - 1\right] \\
& - \frac{\alpha^2 m_W^2}{1536 c_w^4} (\xi_W - 1) D [(\xi_W - 1)^3 (\xi_W^3 - \xi_W^2 - 3\xi_W - 33)c_w^6 \\
& - (\xi_W - 1)(3\xi_W^4 - 9\xi_W^3 - 29\xi_W^2 + 101\xi_W + 366)c_w^4 + (3\xi_W^4 - 10\xi_W^3 - 22\xi_W^2 + 170\xi_W - 93)c_w^2 \\
& - \xi_W^3 + 2\xi_W^2 + 5\xi_W - 18] \theta\left[\frac{1}{c_w} - \sqrt{\xi_W} - 1\right] \\
& - \frac{\alpha^2 m_W^2}{128 s_w^4 \xi_W^2} (1 - 4 c_w^2 \xi_W)^{3/2} \sum_{i=e,\mu,\tau} x_i (x_i - \xi_W)^2 \theta\left[\frac{1}{c_w} - 2\sqrt{\xi_W}\right] \theta[\sqrt{\xi_W} m_W - m_i] \\
& - \frac{3 \alpha^2 m_W^2}{128 s_w^4 \xi_W^2} (1 - 4 c_w^2 \xi_W)^{3/2} \sum_{i=u,c} \sum_{j=d,s,b} |V_{ij}|^2 C_{ij} (\xi_W (x_i + x_j) - (x_i - x_j)^2) \\
& \times \theta\left[\frac{1}{c_w} - 2\sqrt{\xi_W}\right] \theta[\sqrt{\xi_W} m_W - m_i - m_j] + \frac{\alpha^2 m_W^2}{128 c_w^4 s_w^4} (2c_W^2 - 1) \\
& \times \sum_{i=e,\mu,\tau} \frac{1}{x_i} \sqrt{1 - 4 c_w^2 x_i} (x_i - \xi_W)^2 (2c_w^2 - 1 + c_w^2 (4c_w^2 - 5)x_i) \theta[m_i - \sqrt{\xi_W} m_W]
\end{aligned}$$









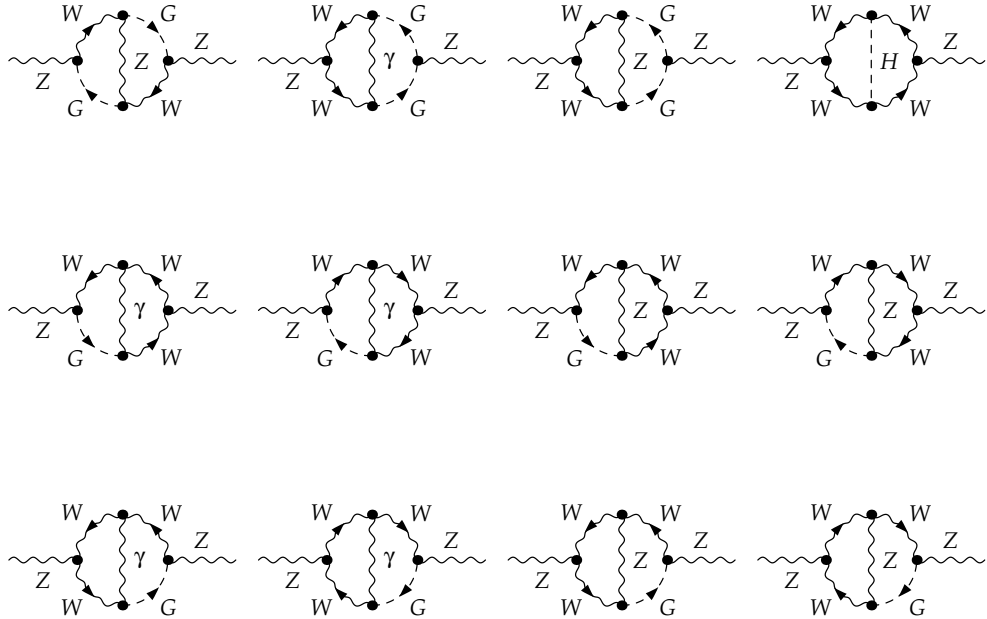


FIG. 13: $Z \xi_W$ -dependent two-loop self-energy diagrams under the 6th topology of Fig.3 which satisfy the cutting conditions of Fig.5.

$$\begin{aligned}
& - \frac{\alpha^2 m_W^2}{384 c_w^4 s_w^4} (4c_w^2 - 1) \sum_{i=u,c} \sum_{j=d,s,b} \frac{1}{x_i} |V_{ij}|^2 C_{ij} \sqrt{1 - 4 c_w^2 x_i} (\xi_W - x_i + x_j) \\
& \times (4c_w^2 - 1 + c_w^2 (8c_w^2 - 11)x_i) \theta[m_i - m_j - \sqrt{\xi_W} m_W] \\
& - \frac{\alpha^2 m_W^2}{384 c_w^4 s_w^4} (2c_w^2 + 1) \sum_{i=u,c} \sum_{j=d,s,b} \frac{1}{x_j} |V_{ij}|^2 C_{ij} \sqrt{1 - 4 c_w^2 x_j} (\xi_W - x_j + x_i) \\
& \times (2c_w^2 + 1 + c_w^2 (4c_w^2 - 7)x_j) \theta[m_j - m_i - \sqrt{\xi_W} m_W]. \tag{20}
\end{aligned}$$

From Fig.5 one readily sees that the 4th and 5th cuts and the second and third cuts are right-and-left symmetric. Through careful calculations we also find the ξ_W -dependent contribution of the 4th and 5th cuts of Fig.5 of the diagrams of Fig.13 to Z two-loop mass counterterm is equal to that of the second and third cuts of Fig.5.

Summing up all of the above results we obtain the gauge dependence of the branch cut of Z mass counterterm under the on-shell mass renormalization prescription (see Eqs.(5,14,16-20))

$$\begin{aligned}
\delta m_Z^2|_{\xi_W-cut} &= \frac{\alpha^2 m_W^2}{1728 c_w^6 s_w^2} \left[9 + 3 \sum_{i=e,\mu,\tau} \sqrt{1 - 4 c_w^2 x_i} (16x_i c_w^6 + (8 - 24x_i)c_w^4 + (7x_i - 12)c_w^2 + 5) \right. \\
&+ \sum_{i=u,c} \sqrt{1 - 4 c_w^2 x_i} (64x_i c_w^6 + (32 - 80x_i)c_w^4 + (7x_i - 40)c_w^2 + 17) \\
&+ \sum_{i=d,s,b} \sqrt{1 - 4 c_w^2 x_i} (16x_i c_w^6 + 8(1 - x_i)c_w^4 - (17x_i + 4)c_w^2 + 5) \Big] \\
&\times \left[2D E \theta \left[\frac{1}{c_w} - \sqrt{\xi_W} - 1 \right] - \frac{1}{s_w^2} (1 - 4 c_w^2 \xi_W)^{3/2} \theta \left[\frac{1}{c_w} - 2\sqrt{\xi_W} \right] \right]. \tag{21}
\end{aligned}$$

According to the above discussion below Eqs.(5) Eq.(21) proves the Z two-loop mass counterterm is gauge dependent under the on-shell mass renormalization prescription. This means the conventional Z on-shell mass definition is gauge dependent.

Then we discuss the gauge dependence of the branch cut of Z two-loop mass counterterm under the pole mass renormalization prescription. The calculations of the branch cut of Z two-loop self energy are same as the case of the

on-shell mass renormalization prescription. The other term in Z two-loop mass counterterm is (see Eqs.(5))

$$\begin{aligned}
m_Z \Gamma_Z \operatorname{Im} \Sigma'_{ZZ}(m_Z^2)|_{\xi_W - \text{cut}} &= \frac{\alpha^2 m_W^2}{1728 c_w^6 s_w^2} \left[9 + 3 \sum_{i=e,\mu,\tau} \sqrt{1 - 4 c_w^2 x_i} (16x_i c_w^6 + (8 - 24x_i)c_w^4 + (7x_i - 12)c_w^2 + 5) \right. \\
&+ \sum_{i=u,c} \sqrt{1 - 4 c_w^2 x_i} (64x_i c_w^6 + (32 - 80x_i)c_w^4 + (7x_i - 40)c_w^2 + 17) \\
&+ \left. \sum_{i=d,s,b} \sqrt{1 - 4 c_w^2 x_i} (16x_i c_w^6 + 8(1 - x_i)c_w^4 - (17x_i + 4)c_w^2 + 5) \right] \\
&\times \left[\frac{1}{s_w^2} (1 - 4 c_w^2 \xi_W)^{3/2} \theta \left[\frac{1}{c_w} - 2\sqrt{\xi_W} \right] - 2D E \theta \left[\frac{1}{c_w} - \sqrt{\xi_W} - 1 \right] \right]. \tag{22}
\end{aligned}$$

According to all the above results we obtain the gauge dependence of the branch cut of Z two-loop mass counterterm under the pole mass renormalization prescription (see Eqs.(5,14,16-20,22))

$$\delta m_Z^2|_{\xi_W - \text{cut}} = 0. \tag{23}$$

This means in Z pole mass definition we don't find the gauge dependence present in Z on-shell mass definition.

From the two-loop W and Z mass counterterms we can calculate the gauge dependence of the two-loop δs_w under the on-shell and pole mass renormalization prescriptions. To two-loop level one has [2]

$$\delta s_w = \frac{c_w^2}{2s_w} \left(\frac{\delta m_Z^2}{m_Z^2} - \frac{\delta m_W^2}{m_W^2} \right) + \frac{c_w^2}{2s_w} \left(\frac{\delta m_Z^2 \delta m_W^2}{m_Z^2 m_W^2} - \frac{(\delta m_Z^2)^2}{m_Z^4} \right) - \frac{c_w^4}{8s_w^3} \left(\frac{\delta m_Z^2}{m_Z^2} - \frac{\delta m_W^2}{m_W^2} \right)^2 + O(g^6). \tag{24}$$

The one-loop W and Z mass counterterms have been proved gauge invariant [6]. So we only need to investigate the gauge dependence of the first term of the r.h.s. of Eq.(24). From Eqs.(11,21) we obtain the gauge dependence of the branch cut of the two-loop δs_w under the on-shell mass renormalization prescription

$$\begin{aligned}
\delta s_w|_{\xi_W - \text{cut}} &= \frac{\alpha^2}{3456 c_w^2 s_w^3} \left[9 + 3 \sum_{i=e,\mu,\tau} \sqrt{1 - 4 c_w^2 x_i} (16x_i c_w^6 + (8 - 24x_i)c_w^4 + (7x_i - 12)c_w^2 + 5) \right. \\
&+ \sum_{i=u,c} \sqrt{1 - 4 c_w^2 x_i} (64x_i c_w^6 + (32 - 80x_i)c_w^4 + (7x_i - 40)c_w^2 + 17) \\
&+ \left. \sum_{i=d,s,b} \sqrt{1 - 4 c_w^2 x_i} (16x_i c_w^6 + 8(1 - x_i)c_w^4 - (17x_i + 4)c_w^2 + 5) \right] \\
&\times \left[2D E \theta \left[\frac{1}{c_w} - \sqrt{\xi_W} - 1 \right] - \frac{1}{s_w^2} (1 - 4 c_w^2 \xi_W)^{3/2} \theta \left[\frac{1}{c_w} - 2\sqrt{\xi_W} \right] \right] + \frac{\alpha^2 c_w^2}{1152 s_w^3} \\
&\times \left[3 \sum_{i=u,c} \sum_{j=d,s,b} |V_{ij}|^2 A_{ij} B_{ij} + \sum_{i=e,\mu,\tau} (1 - x_i)^2 (2 + x_i) \right] (1 - \xi_W) (\xi_W^2 - 2\xi_W - 11) \theta[1 - \xi_W]. \tag{25}
\end{aligned}$$

Similarly Eq.(25) proves δs_w and the s_w definition are gauge dependent under the on-shell mass renormalization prescription. On the other hand, from Eqs.(13,23) we obtain the gauge dependence of the branch cut of the two-loop δs_w under the pole mass renormalization prescription

$$\delta s_w|_{\xi_W - \text{cut}} = 0. \tag{26}$$

This means in s_w pole definition we don't find the gauge dependence present in s_w on-shell definition.

III. GAUGE DEPENDENCE OF PHYSICAL RESULT UNDER THE ON-SHELL MASS RENORMALIZATION PRESCRIPTION

From the above discussions one readily sees that the conventional on-shell mass renormalization prescription is unreasonable. In fact the on-shell mass renormalization condition of Eq.(1) doesn't exist, because only the last term of the l.h.s. of Eq.(1) is gauge dependent (see Eqs.(5,11,21)) and the gauge dependence cannot be cancelled out in the equation, so Eq.(1) doesn't hold true. In this section we will discuss whether the gauge dependence of the on-shell mass definition affects the gauge invariance of physical result.

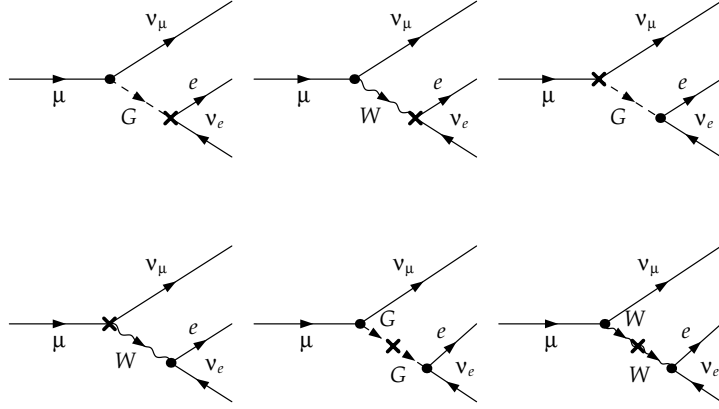


FIG. 14: Diagrams containing the two-loop counterterms δs_w and δm_W^2 of $\mu \rightarrow \nu_\mu e^- \bar{\nu}_e$.

We give the physical process $\mu \rightarrow \nu_\mu e^- \bar{\nu}_e$ as an example to illustrate this problem. Note that we only consider the gauge dependence of the branch cut containing the functions $\theta[1 - \xi_W]$, $\theta[1/c_w - \sqrt{\xi_W} - 1]$ and $\theta[1/c_w - 2\sqrt{\xi_W}]$ of the two-loop cross section of the physical process. This will not break our conclusion. Under the consideration only the diagrams which contain the two-loop counterterms δs_w and δm_W^2 as shown in Fig.14 need to be consider. This is because: 1) all the one-loop physical parameter's counterterms and the other two-loop counterterms of the lepton masses and electron charge don't contain the theta functions $\theta[1 - \xi_W]$, $\theta[1/c_w - \sqrt{\xi_W} - 1]$ and $\theta[1/c_w - 2\sqrt{\xi_W}]$; 2) the total energy in the $\mu \rightarrow \nu_\mu e^- \bar{\nu}_e$ process is order of muon energy which cannot reach the threshold of the branch cut of these theta functions. We can easily obtain the contribution containing the two-loop counterterms δs_w and δm_W^2 of Fig.14 to the physical amplitude $\mu \rightarrow \nu_\mu e^- \bar{\nu}_e$

$$\begin{aligned} \mathcal{M}(\mu \rightarrow \nu_\mu e^- \bar{\nu}_e) \sim & \frac{4\pi\alpha(m_e m_\mu F_1 - m_W^2 F_2)}{m_W^2 s_w^3 (m_W^2 - m_e^2 - 2q_2 \cdot q_3)} \delta s_w + \frac{2\pi\alpha \delta m_W^2}{m_W^4 s_w^2 (m_W^2 - m_e^2 - 2q_2 \cdot q_3)^2} \\ & \times [m_e m_\mu (2m_W^2 - m_e^2 - 2q_2 \cdot q_3) F_1 - m_W^4 F_2], \end{aligned} \quad (27)$$

where m_e and m_μ are the masses of electron and muon, q_2 and q_3 are the momentums of electron and the anti electron neutrino, and

$$F_1 = \bar{u}(q_1) \cdot \gamma_R \cdot u(p) \bar{u}(q_2) \cdot \gamma_L \cdot \nu(q_3), \quad F_2 = \bar{u}(q_1) \cdot \gamma^\mu \cdot \gamma_L \cdot u(p) \bar{u}(q_2) \cdot \gamma_\mu \cdot \gamma_L \cdot \nu(q_3), \quad (28)$$

with p and q_1 the momentums of muon and muon neutrino and γ_L and γ_R the left- and right- handed helicity operators. The two-loop contribution of Eq.(27) to the modulus square of $\mathcal{M}(\mu \rightarrow \nu_\mu e^- \bar{\nu}_e)$ is

$$|\mathcal{M}(\mu \rightarrow \nu_\mu e^- \bar{\nu}_e)|^2 \sim \frac{16\pi^2\alpha^2 q_1 \cdot q_2 (m_e^2 - m_\mu^2 + 2q_1 \cdot q_2)}{m_W^4 s_w^4} \left(\frac{2\delta s_w}{s_w} + \frac{\delta m_W^2}{m_W^2} \right). \quad (29)$$

In Eq.(29) we have averaged the result over the incoming particles' helicity state and summed the result over the outgoing particles' helicity states, and only kept the lowest order of m_e^2/m_W^2 , m_μ^2/m_W^2 and so on since the products of the external-line momentums are very small compared with m_W^2 .

From Eqs.(11,25,29) we obtain the gauge dependence of the branch cut containing the functions $\theta[1 - \xi_W]$, $\theta[1/c_w - \sqrt{\xi_W} - 1]$ and $\theta[1/c_w - 2\sqrt{\xi_W}]$ of the two-loop $|\mathcal{M}(\mu \rightarrow \nu_\mu e^- \bar{\nu}_e)|^2$ under the on-shell mass renormalization prescription

$$\begin{aligned} |\mathcal{M}(\mu \rightarrow \nu_\mu e^- \bar{\nu}_e)|_{\xi_W-cut}^2 \sim & \frac{\pi^2\alpha^4 q_1 \cdot q_2 (m_e^2 - m_\mu^2 + 2q_1 \cdot q_2)}{108m_W^4 c_w^2 s_w^8} \left[9 \right. \\ & + 3 \sum_{i=e,\mu,\tau} \sqrt{1 - 4c_w^2 x_i} (16x_i c_w^6 + (8 - 24x_i)c_w^4 + (7x_i - 12)c_w^2 + 5) \\ & + \sum_{i=u,c} \sqrt{1 - 4c_w^2 x_i} (64x_i c_w^6 + (32 - 80x_i)c_w^4 + (7x_i - 40)c_w^2 + 17) \\ & \left. + \sum_{i=d,s,b} \sqrt{1 - 4c_w^2 x_i} (16x_i c_w^6 + 8(1 - x_i)c_w^4 - (17x_i + 4)c_w^2 + 5) \right] \end{aligned}$$

$$\begin{aligned}
& \times \left[2D E \theta \left[\frac{1}{c_w} - \sqrt{\xi_W} - 1 \right] - \frac{1}{s_w^2} (1 - 4 c_w^2 \xi_W)^{3/2} \theta \left[\frac{1}{c_w} - 2\sqrt{\xi_W} \right] \right] \\
& + \frac{\pi^2 \alpha^4 q_1 \cdot q_2 (m_e^2 - m_\mu^2 + 2q_1 \cdot q_2)}{36 m_W^4 s_w^8} (2c_w^2 - 1)(1 - \xi_W)(\xi_W^2 - 2\xi_W - 11) \\
& \times \left[3 \sum_{i=u,c} \sum_{j=d,s,b} |V_{ij}|^2 A_{ij} B_{ij} + \sum_{i=e,\mu,\tau} (1 - x_i)^2 (2 + x_i) \right] \theta[1 - \xi_W]. \quad (30)
\end{aligned}$$

Since there is no other term to cancel out the gauge dependence of Eq.(30), this result means the on-shell mass renormalization prescription makes the cross section of the physical process $\mu \rightarrow \nu_\mu e^- \bar{\nu}_e$ gauge dependent. We can draw a diagram to show this gauge dependence. In Fig.15 we have used the data: $e = 0.3028$, $s_w^2 = 0.2312$,

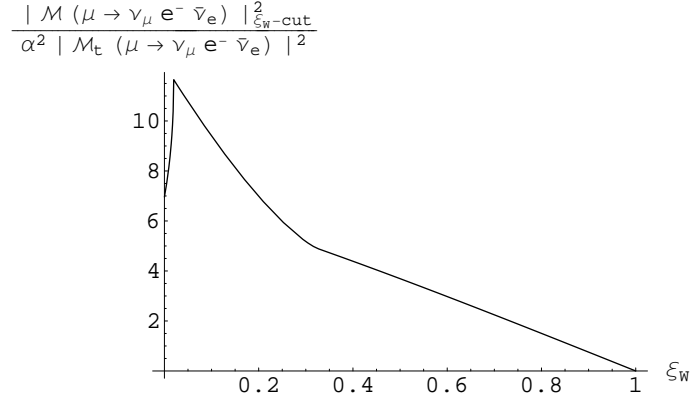


FIG. 15: Gauge dependence of the two-loop $|\mathcal{M}(\mu \rightarrow \nu_\mu e^- \bar{\nu}_e)|^2$ under the on-shell mass renormalization prescription, where $\mathcal{M}_t(\mu \rightarrow \nu_\mu e^- \bar{\nu}_e)$ is the tree-level amplitude and $q_1 \cdot q_2 = q_2 \cdot q_3 = m_\mu^2/6 - m_e^2/2$.

$m_W = 80.42 \text{ GeV}$, $m_u = 3 \text{ MeV}$, $m_c = 1.25 \text{ GeV}$, $m_t = 174.3 \text{ GeV}$, $m_d = 6 \text{ MeV}$, $m_s = 120 \text{ MeV}$, $m_b = 4.2 \text{ GeV}$, $m_e = 0.5110 \text{ MeV}$, $m_\mu = 105.7 \text{ MeV}$, $m_\tau = 1.777 \text{ GeV}$, $|V_{ud}| = 0.975$, $|V_{us}| = 0.223$, $|V_{ub}| = 0.004$, $|V_{cd}| = 0.222$, $|V_{cs}| = 0.974$, $|V_{cb}| = 0.040$, $|V_{td}| = 0.009$, $|V_{ts}| = 0.039$, $|V_{tb}| = 0.999$ [15]. Obviously the gauge dependence of $|\mathcal{M}(\mu \rightarrow \nu_\mu e^- \bar{\nu}_e)|^2$ is $O(1)$ at two-loop level, thus it can not be neglected since the present experiments have researched this precision. On the other hand, from Eqs.(13,26,29) in the pole mass renormalization prescription we don't find such gauge dependence of the physical result present in the on-shell mass renormalization prescription.

IV. CONCLUSION

We have discussed the gauge dependence of W and Z mass definitions under the on-shell and pole mass renormalization prescriptions. Through the calculations of W and Z two-loop mass counterterms we strictly prove that the unstable boson's mass definition is gauge dependent under the on-shell mass renormalization prescription. This leads to the physical result obtained by the on-shell mass renormalization prescription also gauge dependent. On the contrary, we don't find such gauge dependence in the pole mass renormalization prescription. Besides, the difference of the physical result between the two mass renormalization prescriptions cannot be neglected at two-loop level. Therefore we should use the pole mass renormalization prescription rather than the on-shell mass renormalization prescription to calculate physical results beyond one-loop level.

Acknowledgments

The author thanks Prof. Xiao-Yuan Li and Prof. Cai-dian Lu for their useful guidance.

[1] M. Veltman, Physica **29** (1963) 186;

D. Bardin and G. Passarino, The Standard Model in the Making Precision Study of the Electroweak Interactions, Oxford Science Pub., Clarendon Press, Oxford, 1999.

- [2] A. Denner, *Fortschr. Phys.* **41** (1993) 307.
- [3] A. Sirlin, *Phys. Rev. Lett.* **67** (1991) 2127; *Phys. Lett. B* **267** (1991) 240; R.G. Stuart, *Phys. Lett. B* **272** (1991) 353.
- [4] M. Passera, A. Sirlin, *Phys. Rev. Lett.* **77** (1996) 4146; B.A. Kniehl, A. Sirlin, *Phys. Rev. Lett.* **81** (1998) 1373; P.A. Grassi, B.A. Kniehl and A. Sirlin, *Phys. Rev. Lett.* **86** (2001) 389; M.L. Nekrasov, *Phys. Lett. B* **531** (2002) 225; B.A. Kniehl, A. Sirlin, *Phys. Lett. B* **530** (2002) 129.
- [5] J.C. Breckenridge, M.J. Lavelle, T.G. Steele, *Z. Phys. C* **65** (1995) 155.
- [6] P. Gambino, P.A. Grassi, *Phys. Rev. D* **62** (2000) 076002.
- [7] At present a strict proof of the native hypothesis is only present in Ref.[6], but there is a contradiction in the proof which makes the proof invalid, i.e. in order to derive Eq.(18) of Ref.[6] the authors used the conditions $\beta_{MW}^\xi = 0$ and $\delta_t = 0$, but the two conditions are contradictory: when $\delta_t = 0$, one will have $\beta_{MW}^\xi \neq 0$. This contradiction has been discussed in Ref.[6], but the authors are unaware of the gravity of the problem.
- [8] N.K. Nielsen, *Nucl. Phys. B* **101** (1975) 173; R. Tarrach, *Nucl. Phys. B* **183** (1981) 384; O. Piguet and K. Sibold, *Nucl. Phys. B* **253** (1985) 517; N. Gray, D.J. Broadhurst, W. Grafe, K. Schilcher, *Z. Phys. C* **48** (1990) 673; D.J. Broadhurst, N. Gray, K. Schilcher, *Z. Phys. C* **52** (1991) 111.
- [9] J. Kublbeck, M. Bohm, A. Denner, *Comput. Phys. Commun.* **60** (1990) 165; G.J. van Oldenborgh, J.A.M. Vermaelen, *Z. Phys. C* **46** (1990) 425; T. Hahn, M. Perez-Victoria, *Comput. Phys. Commun.* **118** (1999) 153.
- [10] J. Gegelia, G. Japaridze, A. Tkabladze, A. Khelashvili, K. Turashvili, [hep-ph/9910527](#); F. Jegerlehner, M.Yu. Kalmykov and O. Veretin, *Nucl. Phys. B* **641** (2002) 285; F. Jegerlehner, M.Yu. Kalmykov and O. Veretin, *Nucl. Phys. B* **658** (2003) 49.
- [11] A. Freitas, W. Hollik, W. Walter, G. Weiglein, *Phys. Lett. B* **495** (2000) 338; A. Freitas, W. Hollik, W. Walter, G. Weiglein, *Nucl. Phys. B* **632** (2002) 189.
- [12] R.E. Cutkosky, *J. Math. Phys.* **1**, 429 (1960).
- [13] Y. Zhou, [hep-ph/0508225](#).
- [14] N. Cabibbo, *Phys. Rev. Lett.* **10**, 531 (1963); M. Kobayashi and K. Maskawa, *Prog. Theor. Phys.* **49** (1973) 652.
- [15] The European Physical Journal C, **15** (2000) 1-878.